JGR Space Physics

RESEARCH ARTICLE
10.1029/2023JA031699

Key Points:

- 2-D hybrid simulations are performed to study the formation of downstream high-speed jets (HSJs) and ripples in quasi-parallel shocks due to the interaction between upstream structures and the shock front
- In a parallel shock, the shock ripples remain in the same regions of the shock front, and large-scale HSJs can form downstream of the ripples
- In a quasi-parallel shock, the shock ripples move along the shock front and the downstream HSJs become smaller as the shock angle increases

Correspondence to:

Q. Lu,
qmlu@ustc.edu.cn

Citation:

Ren, J., Lu, Q., Guo, J., Gao, X., Lu, S., Wang, S., & Wang, R. (2023). Two-dimensional hybrid simulations of high-speed jets downstream of quasi-parallel shocks. *Journal of Geophysical Research: Space Physics*, *128*, e2023JA031699. https://doi.org/10.1029/2023JA031699

Received 15 MAY 2023
Accepted 13 AUG 2023

Author Contributions:

Conceptualization: Junyi Ren, Quanming Lu
Data curation: Junyi Ren
Formal analysis: Junyi Ren
Funding acquisition: Quanming Lu
Investigation: Junyi Ren
Project Administration: Quanming Lu
Software: Junyi Ren, Quanming Lu
Supervision: Quanming Lu, Xinliang Gao
Validation: Jin Guo
Visualization: Junyi Ren
Writing – original draft: Junyi Ren
Writing – review & editing: Quanming Lu, Jin Guo, Xinliang Gao, San Lu, Shimou Wang, Rongsheng Wang

© 2023. American Geophysical Union. All Rights Reserved.

Two-Dimensional Hybrid Simulations of High-Speed Jets Downstream of Quasi-Parallel Shocks

Junyi Ren[1,2], Quanming Lu[1,2,3], Jin Guo[1,2], Xinliang Gao[1,2,3], San Lu[1,2,3], Shimou Wang[1,2,3], and Rongsheng Wang[1,2,3]

[1]Deep Space Exploration Laboratory/School of Earth and Space Sciences, University of Science and Technology of China, Hefei, China, [2]CAS Center for Excellence in Comparative Planetology/CAS Key Lab of Geospace Environment, University of Science and Technology of China, Hefei, China, [3]Collaborative Innovation Center of Astronautical Science and Technology, Harbin, China

Abstract High-speed jets (HSJs) are frequently observed downstream of a quasi-parallel bow shock, and they are considered to play important roles in the coupling of the solar wind, the magnetosheath, and the magnetosphere. Using two-dimensional hybrid simulations, we study the formation of HSJs in quasi-parallel shocks with different shock angles (θ_{Bn}). The interaction of the upstream compressive structures that are inhomogeneous in the direction perpendicular to the background magnetic field and the shock front leads to the shock ripples, and then the downstream HSJs. In a parallel shock with the shock angle $\theta_{Bn} = 0°$, the interaction regions of the upstream compressive structures with the shock front don't change with time. The shock ripples remain in the same regions of the shock front, and then the HSJs can develop into large-scale sizes, especially under low plasma β or high Mach number (M_A). While in a quasi-parallel shock with a non-zero shock angle, the interaction regions of the upstream compressive structures with the shock front move along the shock front. The shock ripples change with time, and the scale size of the downstream HSJs becomes smaller with the increase of the shock angle.

1. Introduction

Collisionless shocks have significant roles in space and astrophysical plasmas, and their behaviors are mainly controlled by the angle (θ_{Bn}) between the shock normal and the upstream magnetic field. In a quasi-perpendicular shock where $\theta_{Bn} \gtrsim 45°$, there is a well-defined magnetic field profile, and the ions reflected by the shock usually cannot travel far upstream (Bale et al., 2005; Lembege & Savoini, 1992; Lembege et al., 2004; Leroy et al., 1981; Yang et al., 2009, 2012). When $\theta_{Bn} \lesssim 45°$, the shock is quasi-parallel. Ions reflected by quasi-parallel shocks can travel far upstream along the magnetic field and interact with the solar wind plasma, which generate ion beam instabilities and excite ultra-low-frequency (ULF) waves (Cao et al., 2009; Fu et al., 2009; Hao et al., 2021; Lembege et al., 2004; Q. Lu et al., 2020; Omidi, 2007; Quest, 1988; Su et al., 2012; Wu et al., 2015). The non-linear evolution of the ULF waves leads to various foreshock transient structures, such as short large-amplitude magnetic structures (SLAMS) (Schwartz & Burgess, 1991), foreshock cavitions (Blanco-Cano et al., 2009; Omidi, 2007), spontaneous hot flow anomalies (Omidi et al., 2013; Zhang et al., 2013), etc. The convection of these foreshock structures to the downstream causes the magnetosheath to become turbulent.

One of the interesting phenomena in the turbulent magnetosheath downstream of a quasi-parallel shock is high-speed jets (HSJs). HSJs are plasma flows with enhanced dynamic pressure, and they were first observed in the Earth's magnetosheath by Němeček et al. (1998), referred to as "transient flux enhancements." Plasma flow inside HSJs is often super-Alfvénic, while the temperature is reduced (Archer & Horbury, 2013; Archer et al., 2012; Plaschke et al., 2013, 2018). The magnetic field inside HSJs can be either increasing or decreasing, and the increases of magnetic field are often associated with density enhancement (Archer & Horbury, 2013). Hietala et al. (2009) suggested that HSJs are formed locally by the rippled geometry of the shock front. According to the Rankine-Hugoniot jump condition, upstream plasma flow is deflected and suffers less deceleration when crossing through the inclined part of a rippled shock. As a result, the flow is concentrated onto the dented part and compressed to form an HSJ. This scenario is supported by hybrid simulations (Hao, Lembege, et al., 2016; Preisser et al., 2020), and Hao, Lu, et al. (2016) further concluded that ions are more easily transmitted through the ripple dents because of the interaction between the upstream waves and the shock front. Karlsson et al. (2015) proposed that HSJs are generated by SLAMSs, a kind of upstream compressive structures with enhanced field magnitude and dynamic pressure. When the SLAMSs or other similar compressive structures penetrate through a dented part of the shock front, they maintain a higher dynamic pressure than the surrounding plasma and become HSJs (Palmroth et al., 2018; Suni et al., 2021). Other foreshock structures, for example, SHFAs (Omidi et al., 2016), and solar wind discontinuities (Archer et al., 2012; Savin et al., 2012), are also potential sources of HSJs. Recently, Raptis et al. (2022) reported an in-situ observation of the formation process of an HSJ. They conclude that the HSJ can be directly generated from the shock reforming process as the waves pile up between the old and the new shock fronts and are convected downstream.

The scale size of HSJs is usually around 1 R_E or 70 d_i (under average solar wind conditions), where R_E is the Earth radius and d_i is the ion inertial length (Plaschke et al., 2016, 2020), and their maximum size can be up to 5 R_E (350 d_i) (Gunell et al., 2014). HSJs play an important role in the coupling of the solar wind, the magnetosheath, and the magnetosphere. HSJs can lead to the local electron heating (Liu et al., 2019), large-scale HSJs with scale sizes up to several R_E can directly impact the magnetopause and subsequently cause the inward movement of the magnetopause (Archer et al., 2012; Hietala et al., 2009, 2012). The compression of the magnetopause can trigger ULF magnetopause waves (Hietala et al., 2012), and can be accompanied by localized aurora brightening (Han et al., 2016, 2017; Wang et al., 2018). Recently, by performing global hybrid simulations, Guo et al. (2022) found that large-scale HSJs with scale sizes over 2 R_E are only formed downstream of the quasi-parallel shock with the shock angle $\theta_{Bn} = 0°$. However, how the shock angle θ_{Bn} impacts the characteristics of HSJs remains unclear.

In this study, we perform local two-dimensional (2-D) hybrid simulations to investigate the formation of HSJs and ripples in quasi-parallel shocks with different shock angles θ_{Bn}. Our results show that HSJs are formed through the interaction between compressive structures in the upstream and the shock front, and these compressive structures are inhomogeneous in the direction perpendicular to the upstream magnetic field, which makes the scale sizes of the HSJs largely dependent on the shock angle θ_{Bn}. The simulation model is briefly described in Section 2, the simulation cases with different θ_{Bn}, Alfvén Mach number M_A, and plasma β are compared in Section 3, and the conclusions are summarized in Section 4.

2. Simulation Model

In this study, a 2-D hybrid model is used to study the characteristic of HSJs downstream of quasi-parallel shocks with different shock angles θ_{Bn}, Alfvén Mach number M_A, and plasma β. In hybrid simulations, ions are treated as macro-particles so that their full kinetic properties are resolved, while electrons are treated as massless fluid. Because the downstream HSJs are ion scale structures (Hietala et al., 2009), their physics can be resolved by a hybrid simulation model. The developed code based on the model has been effectively utilized to study collisionless shocks (Hao, Lembege, et al., 2016; Hao, Lu, et al., 2016) and low-frequency electromagnetic waves (Q. M. Lu et al., 2006). The simulations are carried out in the x-y plane, with the box size of $L_x \times L_y = 1{,}024\ d_i \times 384\ d_i$, using a grid number of $2{,}048 \times 768$, so that the grid size is $\Delta x = \Delta y = 0.5\ d_i$. Initially, an average of 100 particles exist per grid cell. The left and right x boundaries are set to be reflective and open for particles, respectively, and the electromagnetic fields at both x boundaries are set to be fixed values based on the Rankine-Hugoniot condition. Meanwhile, the y boundaries for both fields and particles are periodic. At the initial state, a uniform magnetic field $\mathbf{B}_0$ is set to lie inside the simulation plane, with its angle to the x-axis set to θ_{Bx}. Furthermore, the densities of ions and electrons are also initiated uniformly, that is, $n_i = n_e = n_0$. The plasma is injected into the domain from the right boundary with a velocity V_{in}, and reflected by the left boundary. The interaction of the reflected plasma with the injected plasma leads to the formation of a shock wave that propagates along the $+x$ direction. In general the shock normal is parallel to the x axis, so $\theta_{Bn} = \theta_{Bx}$. The chosen time step in the simulations is $\Delta t = 0.01\ \ \Omega_i^{-1}$, where Ω_i represents the upstream angular ion cyclotron frequency.

3. Simulation Results

At the Earth's orbit, the solar wind Mach number usually ranges from 1.5 to 15 while is about 7.7 under the average condition, and plasma β can range from 0.01 to 10 with a median value of 0.48 (Veselovsky et al., 2010). Within these ranges, we set up eight cases with different θ_{Bn}, inject velocity V_{in}, and plasma β values. Once fully developed, the shock fronts propagate at an almost constant velocity V_{sh}, so the Mach number can be calculated as $M_A = (V_{\text{sh}} - V_{\text{in}})/V_{A0}$, where V_{A0} is the upstream Alfvén speed. Table 1 shows the simulation configurations together with the calculated Mach numbers. In the simulations, the initial and injected plasma β is isotropic and is

10.1029/2023JA031699

Table 1
Simulation Cases Setups and the Calculated Mach Numbers

Case	1	2	3	4	5	6	7	8
θ_{Bn}	0°	10°	20°	30°	0°	30°	0°	30°
$-V_{\mathrm{in}}/V_{A0}$	6	6	6	6	6	6	4	4
β	0.3	0.3	0.3	0.3	0.03	0.03	0.3	0.3
M_A	7.3	7.3	7.4	7.4	7.3	7.4	4.9	5.0

adjusted by setting the plasma temperature. In the following sub-sections, we will first investigate the formation and evolution of large-scale HSJs in Case 1, and compare it with the other cases to examine the effect of the upstream conditions.

3.1. The Formation of Large-Scale HSJs in Case 1

We first focus on Case 1, in which large-scale HSJs are observed. Figure 1 plots the dynamic pressure $P_d = n(V_{\mathrm{sh}} - V_i)^2$ (Figures 1a–1d), the total magnetic field B (Figures 1e–1h), and the ion temperature T_i (Figures 1i–1l) of Case 1 at $t = 250$, 300, 350, and 400 Ω_i^{-1}. In Figure 1, the shock front (denoted by the white lines) is identified as the position with the maximum gradient of the ion bulk velocity in the x direction V_{ix} along the same y coordinate. The boundaries of HSJs are defined at where the dynamic pressure is equal to half of the upstream value, $P_{d0} = n_0(V_{\mathrm{sh}} - V_{\mathrm{in}})^2$ (Palmroth et al., 2018; Plaschke et al., 2013), and they are denoted by the pink lines. HSJs begin to form just downstream at about $t = 250$ Ω_i^{-1} and their sizes are approximately 50 d_i. In the upstream region, there are plasma waves that propagate parallel to the background magnetic field, which have been extensively investigated by previous studies (e.g., Hao et al., 2021; Quest, 1988; Wu et al., 2015). The waves are excited through ion-beam instabilities triggered by shock-reflected ions, and they are amplified and become

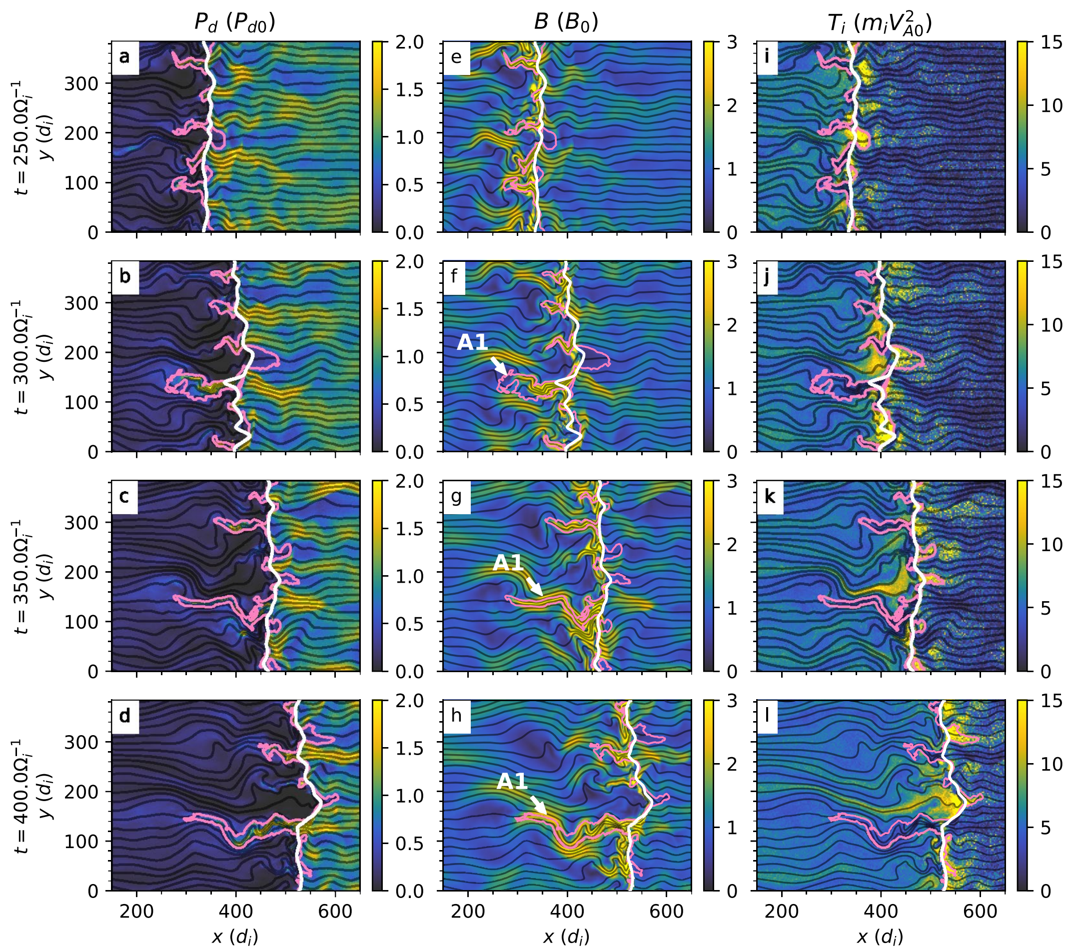

Figure 1. Evolution of the shock in Case 1: (a–d) dynamic pressure $P_d = n(V_{\mathrm{sh}} - V_i)^2$ normalized by the upstream value $P_{d0} = n_0(V_{\mathrm{in}} - V_{\mathrm{sh}})^2$, (e–h) total magnetic field B normalized by upstream magnetic field B_0, and (i–l) ion temperature T_i normalized by $m_i\left(V_{A0}^2\right)$. The black lines in the figure represent the magnetic field lines, and the white and pink lines denote the shock front and the boundaries of high-speed jets respectively.

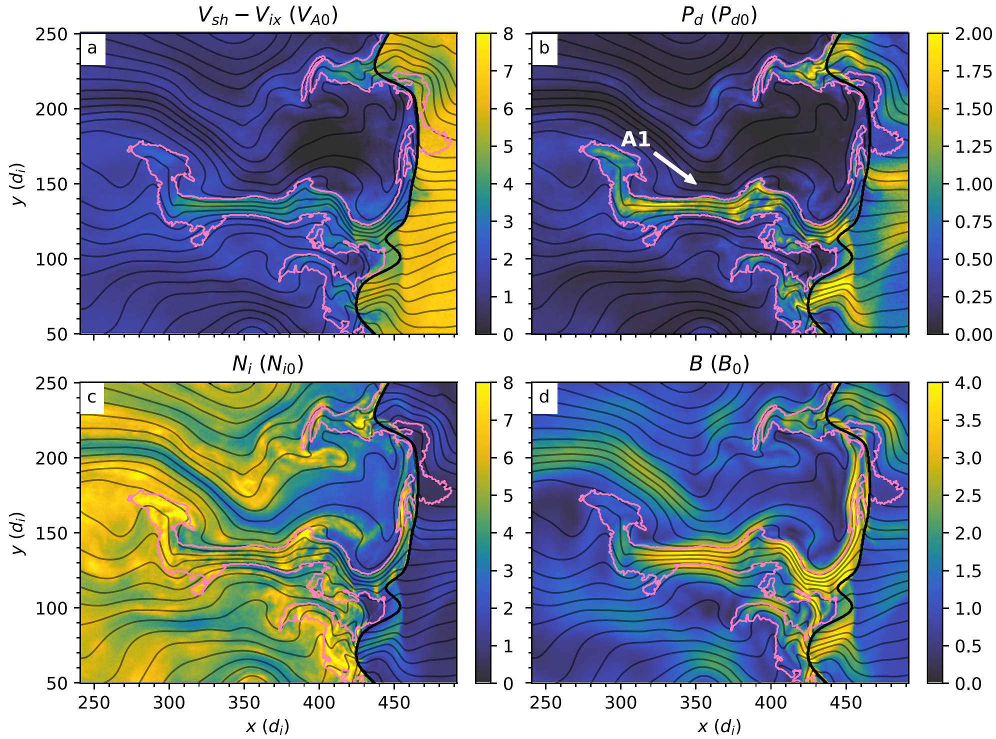

Figure 2. Enlarged view of A1 $t = 320\ \Omega_i^{-1}$ in Case 1. In the panels, we plot (a) x component of the ion bulk velocity in the shock's frame $V_{sh} - V_{ix}$, (b) dynamic pressure P_d, (c) ion density N, and (d) total magnetic field B. The quantities are normalized in the same way as in Figure 1 and N is normalized by upstream value N_0. The black lines represent the magnetic field lines, and the shock front and the boundaries of high-speed jets are denoted by the white and pink lines respectively.

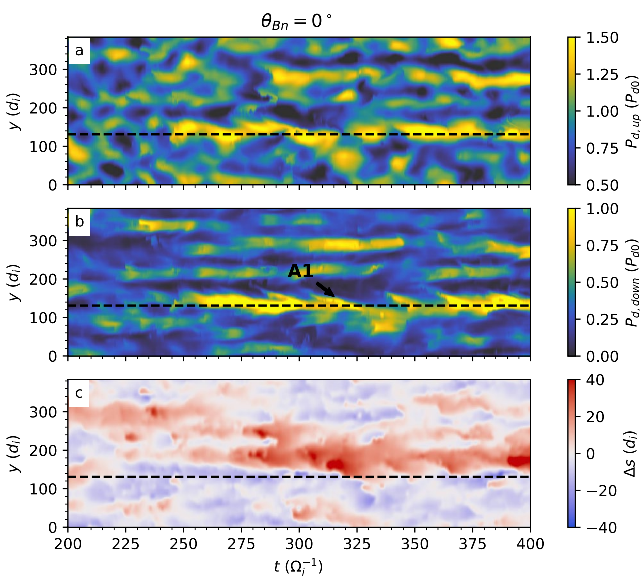

Figure 3. Time evolution in Case 1 of the dynamic pressure P_d averaged in a 30 $d_i \times 30$ d_i box with the center (a) 50 d_i upstream ($P_{d,\mathrm{up}}$, normalized by P_{d0}) from and (b) 20 d_i downstream ($P_{d,\mathrm{down}}$, normalized by P_{d0}) from the identified shock front, and the offset (Δs, in d_i) of the shock front, which is calculated by the distance between the shock front and its average x position. The dashed lines denote the position of high-speed jets A1 in Figure 1.

compressional as they are brought back to the shock by the upstream flow (Scholer, 2003; Tsubouchi & Lembège, 2004). The waves finally evolve into compressive structures with a localized enhancement of density and magnetic field, such as shocklets, SLAMS, long pulsations, etc (Schwartz, 1991). For simplicity, these structures are collectively referred to as "compressive structures" in this study. Interaction of these structures with the shock front results in evident ripple-dents on the shock front, leading to the development of downstream HSJs. At $t = 400\ \Omega_i^{-1}$, the scale size of HSJ A1 (around $y = 130$ d_i) has grown to over 200 d_i. Figure 2 provides an enlarged view of HSJ A1 at $t = 320\ \Omega_i^{-1}$. At the inclined part of the rippled shock front, the plasma flow is deflected toward the HSJ (Figure 2a), consistent with the scenario described by Hietala et al. (2009). Inside the HSJs, the ion bulk speed is super-magnetosonic and greater than those in the surrounding regions, accompanied by enhancement of magnetic field and density, in agreement with satellite observations (e.g., Karlsson et al., 2015).

To give a clearer view of the development of the HSJs, Figure 3 plots the evolution of the upstream dynamic pressure $P_{d,\mathrm{up}}$, the downstream dynamic pressure $P_{d,\mathrm{down}}$, and the shock front offset Δs. Here, the upstream dynamic pressure $P_{d,\mathrm{up}}$ and the downstream dynamic pressure $P_{d,\mathrm{down}}$ are defined as the dynamic pressure averaged in a 30 $d_i \times 30$ d_i box with the center 50 d_i away from the shock front in the upstream and 20 d_i downstream, respectively. Such a kind of averaging process filters out the small-size HSJs, leaving only the large and strong ones. The shock front offset Δs is calculated as $s - s_{\mathrm{av}}$, where s is the position of the shock front and s_{av} is the averaged position of the shock front along the y direction. Therefore, the shock front is convex

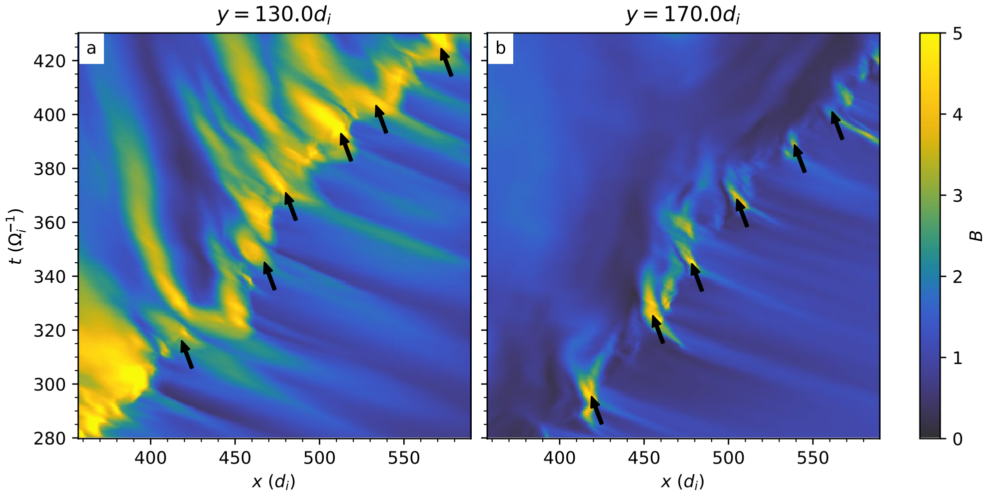

Figure 4. Evolution of total magnetic field B at (a) $y = 130\ d_i$, where high-speed jet (HSJ) A1 is located at, and (b) $y = 170\ d_i$, where no large-scale HSJ presents, in Case 1. The black arrows denote the reformation events.

when Δs is positive, and it is dented when Δs is negative. Obviously, the dynamic pressure in the upstream and downstream have a good correlation, and the HSJs with the enhanced dynamic pressure appear downstream of the dented parts of the rippled shock front. Therefore, the interactions between the compressive structures inhomogeneous along the y direction in the upstream and the shock front lead to the rippled shock front and HSJs in the downstream with the enhanced dynamic pressure. This can be clearly demonstrated by following the time evolution of HSJ A1 (denoted by the dashed line). Here, the y position of the compressive structures in the upstream, the dented part of the rippled shock front, and HSJs in the downstream almost don't change with time.

Raptis et al. (2022) suggested that HSJs can be generated through the shock reformation process, in which the upstream waves pile up between the old and new shock fronts and are convected downstream. However, the large-scale HSJs in this simulation can sustain multiple reformation cycles. Figure 4 plots the total magnetic field as $y = 130\ d_i$, where HSJ A1 is present, and $y = 150\ d_i$, where no large-scale HSJs are visible. At both positions, the reformation cycle period is around 20 Ω_i^{-1}, while HSJ A1 persists for over 150 Ω_i^{-1} throughout the exhibited time interval, and no significant HSJ forms during the reformation cycles at $y = 170\ d_i$. Therefore, the large-scale HSJs in this simulation are not direct results of the shock reformation process.

3.2. The Movement of Compressive Structures With Non-Zero θ_{Bn}

Then we examine the evolution of HSJs in shocks with different θ_{Bn}. In Cases 2–4, θ_{Bn} are set to 10°, 20°, and 30°, respectively, while the other parameters are kept the same as Case 1. Figure 5 plots the dynamic pressure $P_d = n(V_{\mathrm{sh}} - V_i)^2$ (Figures 5a–5d), the total magnetic field B (Figures 5e–5h), and the ion temperature T_i (Figures 5i–5l) of Case 4 at $t = 270$, 300, 330, and 360 Ω_i^{-1}. The position of the shock front and the boundaries of HSJs are plotted using the same method as in Figure 1. Compared to Case 1, both the scale size and strength of the HSJs are smaller, and the shock ripples are also less obvious. There are also compressive structures in the upstream region of the shock front, characterized by enhanced dynamic pressure P_d and magnetic field B, which extend along the upstream background magnetic field. Similar to Case 1, when these upstream compressive structures interact with the shock front, the shock front becomes dented, and HSJs are formed just downstream of the dented part of the shock front, extending almost along the downstream magnetic field.

To investigate why HSJs do not evolve into large-scale sizes in Case 4, we first study the evolution of HSJ B2 in detail. Figure 6 shows the x component of the ion bulk velocity in the shock's frame $V_{\mathrm{sh}} - V_{ix}$ and dynamic pressure P_d at $t = 315$, 325, 335, and 345 Ω_i^{-1}. At $t = 315$ Ω_i^{-1}, HSJ B2 is small, with a size about 10 d_i, located around $y = 250\ d_i$. As time progresses, the shock front at $y = 250\ d_i$ starts to dent downstream, and HSJ B2 becomes more apparent. In the upstream region corresponding to HSJ B2, there is a compressive structure with enhanced dynamic pressure denoted as "CS1," aligned almost parallel to the magnetic field. HSJs result from the interaction between the compressive structure and the shock front. Structure CS1 propagates along the magnetic

10.1029/2023JA031699

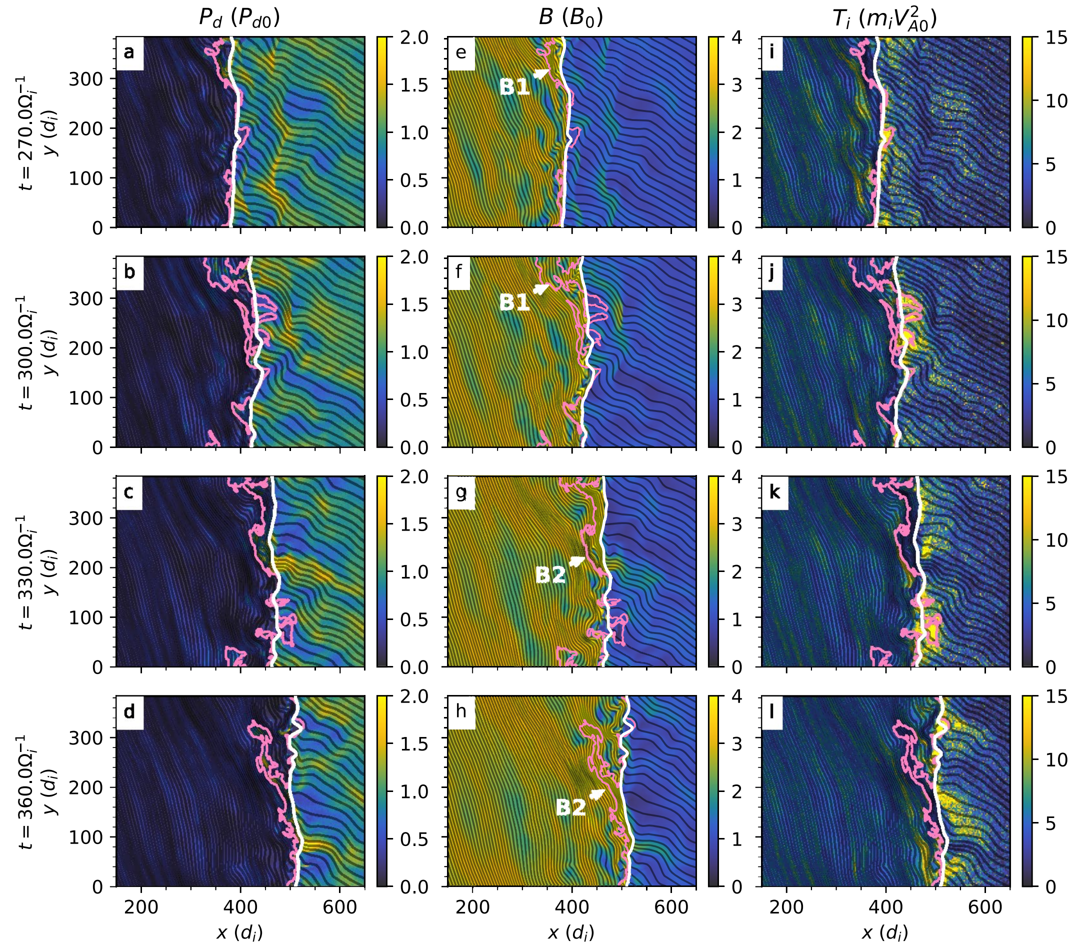

Figure 5. Evolution of the shock in Case 4 shown by (a–d) the dynamic pressure P_d, (e–h) the total magnetic field B, and (i–l) the ion temperature T_i. The quantities are in the same way as in Figure 1. The black lines in the figure represent the magnetic field lines, and the white and pink lines denote the shock front and the boundaries of high-speed jets respectively.

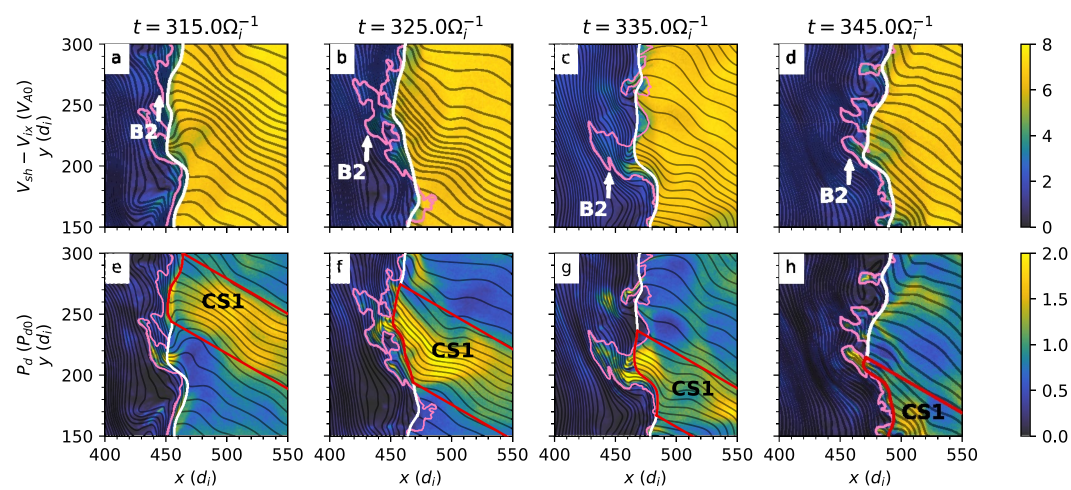

Figure 6. Evolution of high-speed jet B2 in Figure 5, Case 4. (a–d) The x component of the ion bulk velocity in the shock's frame $V_{\mathrm{sh}} - V_{ix}$, (e–h) the dynamic pressure P_d. The red lines encircle the compressive structure CS1.

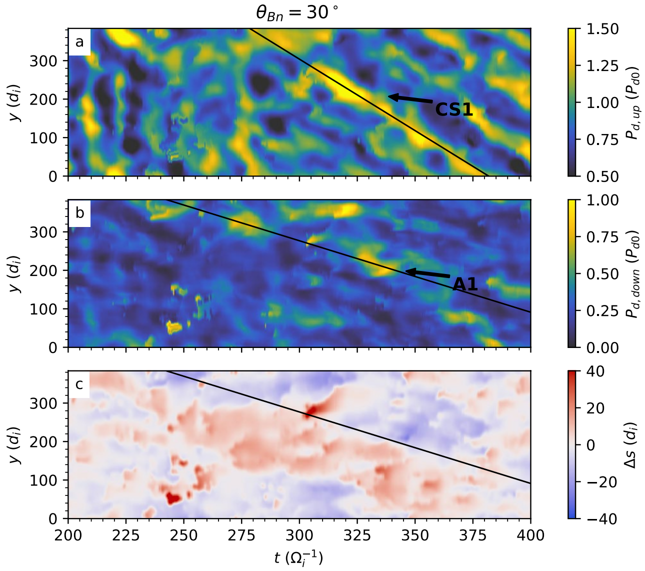

Figure 7. Time evolution of the dynamic pressure averaged in a 30 $d_i \times 30$ d_i box with the center (a) 50 d_i upstream ($P_{d,\mathrm{up}}$) and (b) 20 d_i downstream ($P_{d,\mathrm{down}}$) from the identified shock front, and the offset (Δs) of the shock front of Case 4. The quantities are normalized the same as in Figure 3. The black reference line in panel (a) shows the movement of the compressive structure CS1, and the slope of the line is $k = -4.29$ V_{A0}. In panels (b) and (c) the black reference lines show the movement of high-speed jets and shock ripples, and the slope of the lines is $k = -2.1$ V_{A0}.

field away from the shock front at a velocity of about V_{A0}, while the upstream plasma flow brings it back toward the shock front along the x direction at a velocity of about 6 V_{A0}. In the presence of a non-zero shock angle θ_{Bn}, as shown in the figure, the upstream structure CS1 moves toward the lower-left direction. As a result, the interaction region of the structure CS1 and shock front moves downwards along the shock front. Simultaneously, HSJ B2 in the downstream also moves downwards. At $t = 335$, the dented part of the shock front corresponding to the HSJ B2 is about 20 d_i to the left of the convex part, and the size of B2 is about 100 d_i. When the interaction region of the compressive structure leaves the root of HSJ B2, the HSJ starts to dissipate and its size decreases accordingly. Other HSJs exhibit similar evolutions.

To show the movement of the compressive structures, the shock ripples, and downstream HSJs more clearly, Figure 7 illustrates the evolution of the upstream dynamic pressure $P_{d,\mathrm{up}}$, the downstream dynamic pressure $P_{d,\mathrm{down}}$, and the shock front offset Δs. The upstream and downstream dynamic pressure $P_{d,\mathrm{up}}$ and $P_{d,\mathrm{down}}$ are defined as the average dynamic pressure in a 30 $d_i \times 30$ d_i box centered at 50 d_i and 20 d_i away from the shock front in the upstream and downstream, respectively, consistent with Figure 3. From Figure 7, it is observed that the upstream compressive structures, shock ripples, and downstream HSJs move obviously toward the bottom. The upstream compressive structures move faster with a velocity of about 4.29 V_{A0}, while the velocity of the shock ripples and downstream HSJs is about 2.1 V_{A0}. This difference indicates that the formation of shock ripples is delayed after the upstream compressive structures interact with the shock front. Additionally, the downstream bulk velocity, averaged in t = 300-400 Ω_i^{-1} between 200 and 50 d_i downstream of the shock front, is about 0.20 V_{A0} in the $+y$ direction. This result agrees with the prediction value of 0.24 V_{A0} by Rankine-Hugoniot conditions. Apparently, the downstream bulk velocity is much smaller than the speeds along the shock front of both the upstream compressive structures and the downstream HSJs, and its effect on the evolution of HSJs can therefore be neglected.

Figure 8 shows the dynamic pressure in both Cases 2 and 3. Compared with Case 1 and Case 4, it is clear that with the increase of the shock angle θ_{Bn}, the sizes and strengths of downstream HSJs become smaller and smaller.

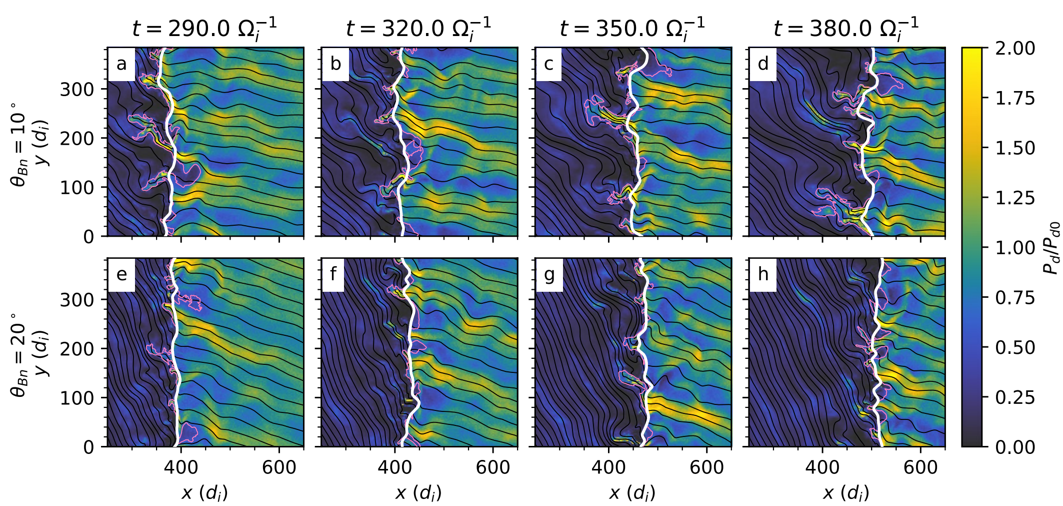

Figure 8. Dynamic pressure P_d of (a–d) Case 3 and (e–h) Case 4 at t = 90, 320, 350, and 380 Ω_i^{-1}. The black lines represent the magnetic field lines, and the white and pink lines denote the shock front and the boundaries of the high-speed jets, respectively.

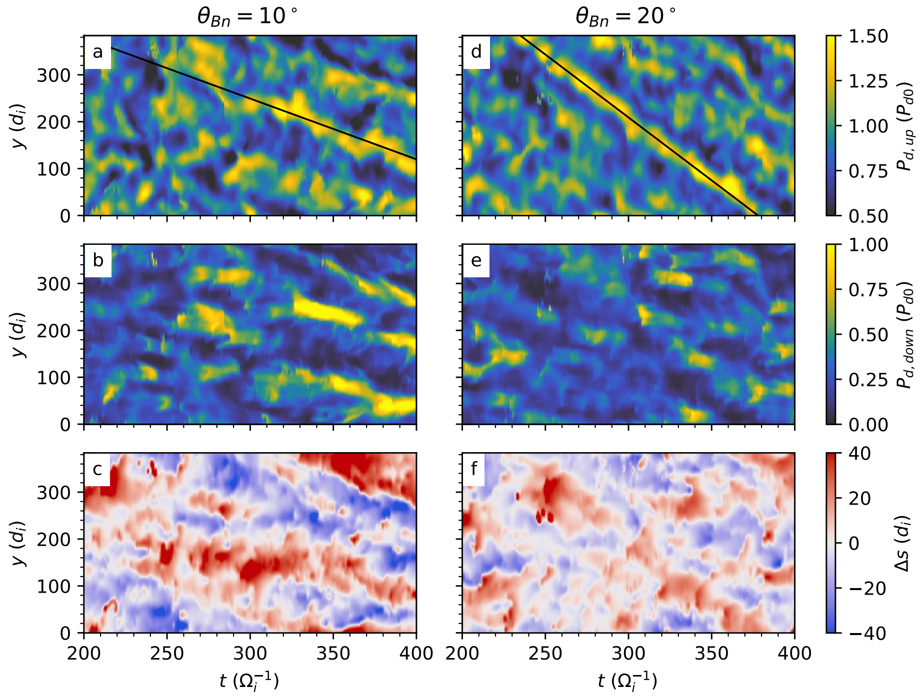

Figure 9. Time evolution of the dynamic pressure averaged in a 30 $d_i \times 30$ d_i box with the center (a, d) 50 d_i upstream ($P_{d,\mathrm{up}}$) and (b, e) 20 d_i downstream ($P_{d,\mathrm{down}}$) from the shock front, and (c, f) the offset (Δs) of the shock front, obtained from (a–c) Case 3 and (d–f) Case 4. The quantities are normalized the same as in Figure 3. The black reference lines show the movement of the compressive structures (a, d).

When $\theta_{Bn} = 10°$ in Case 2, the sizes of the HSJs are about 100 d_i, while the sizes of the HSJs are about 50 d_i at $\theta_{Bn} = 20°$ in Case 3.

Figure 9 shows the evolution in Case 2 and 3 of the upstream dynamic pressure $P_{d,\mathrm{up}}$, the downstream dynamic pressure $P_{d,\mathrm{down}}$, and the shock front offset Δs, which are calculated with the method in Figure 3. Similar to Case 4, the upstream compressive structures, shock ripples, and downstream HSJs propagate toward the bottom, and the propagation speed of the upstream compressive structures is larger than that of both shock ripples and downstream HSJs. Also, with the increase of the shock angle θ_{Bn}, the corresponding propagation speed becomes larger. When $\theta_{Bn} = 10°$, the propagation speed of the upstream compressive structures is about $1.12V_{A0}$, while that of the shock ripples and downstream HSJs is about $0.56V_{A0}$. When $\theta_{Bn} = 20°$, the corresponding speed values are 2.32 V_{A0} and 1.16 V_{A0}, respectively.

3.3. The Effect of Plasma β and Mach Number M_A

Figure 10 shows the time evolution of the upstream/downstream dynamic pressure and the shock front offset for Cases 5 and 6 following in the same format as the previous figures. The plasma β for both cases is reduced to 0.03, and the other parameters remain identical to Cases 1 and 4. As shown in Figures 10a–10c, in Case 5, the y position of the upstream compressive structures and the shock ripples barely change. Although the downstream HSJs exhibit slow movement over time, they still appear within specific y ranges, with the maximum scale size exceeding 200 d_i. Furthermore, the depth of the shock ripples and the strength of the HSJs are higher than those in Case 1 due to the slower dissipation with a lower temperature. In Case 6 (Figures 10d–10f), where $\theta_{Bn} = 30°$, the upstream compressive structures move along the shock front with almost the same speed as the HSJs, while no clear movement pattern is evident in the shock front ripples. Similar to Case 2, the maximum scale size of the HSJs in Case 6 is within 100 d_i.

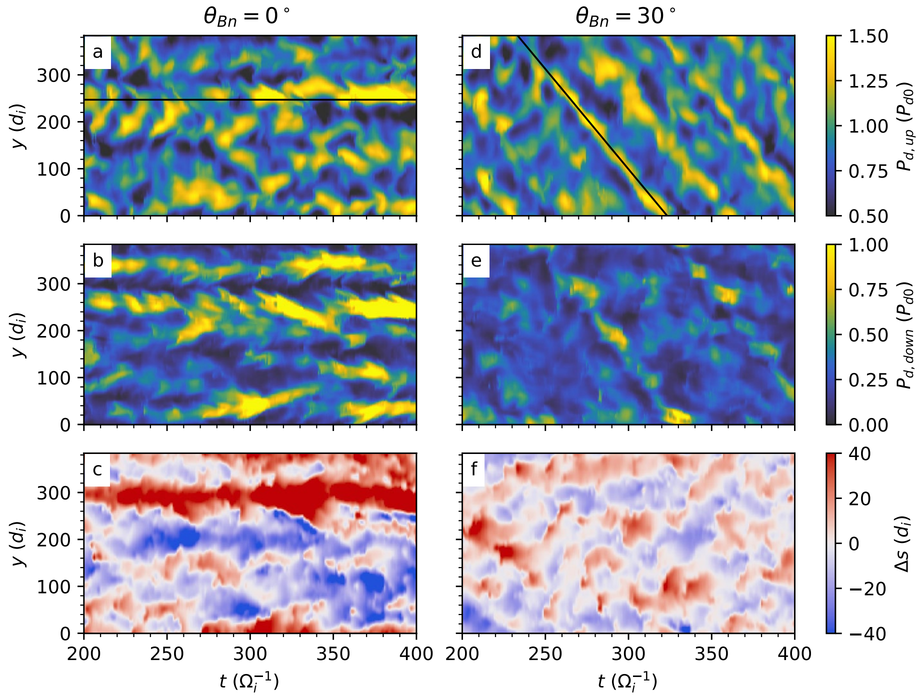

Figure 10. Time evolution of the dynamic pressure averaged in a 30 d_i × 30 d_i box with the center (a, d) 50 d_i upstream ($P_{d,\mathrm{up}}$) and (b, e) 20 d_i downstream ($P_{d,\mathrm{down}}$) from the shock front, and (c, f) the offset (Δs) of the shock front, obtained from (a–c) Case 5 and (d-f) Case 6. The quantities are normalized the same as in Figure 3. The black reference lines show the movement of the compressive structures (a, d).

The time evolution of the upstream/downstream dynamic pressure and the shock front offset, as defined in Section 3.1 for Cases 7 and 8, is shown in Figure 11. In both cases, the velocity of injected plasma is reduced to 4 V_{A0}, and the Mach number is decreased to around 5, while other parameters are kept identical to Cases 1 and 4. The upstream compressive structures, the HSJs, and the shock front ripples move in a similar manner to Cases 1 and 2; however, their magnitude and depth are lower than those in the corresponding cases with higher Mach numbers. As a result, the scale sizes of HSJs are smaller, with a maximum of around 80 d_i in Case 7 and 30 d_i in Case 8. Note that the scale sizes of the HSJs when $\theta_{Bn} = 30°$ are still smaller than those when $\theta_{Bn} = 0°$ due to the movement of the interaction regions of the compressive structures and the shock front.

4. Conclusions and Discussion

In this paper, we study the formation of HSJs in parallel and quasi-parallel shocks by performing 2-D hybrid simulations. The conclusions are summarized as follows:

1. The interaction between the upstream compressive structures and the shock front leads to the shock ripples and HSJs just downstream of the dented parts of the shock front.
2. At a parallel shock ($\theta_{Bn} = 0°$), the interaction regions between the upstream compressive structures and the shock front remain unchanged, and the downstream HSJs can grow into large scales. The scale sizes of HSJs can become larger with the decreasing plasma β.
3. At a quasi-parallel shock with a finite shock angle θ_{Bn}, the interaction regions between the upstream compressive structures and the shock front move along the shock front, and the downstream HSJs also propagate along the y direction.

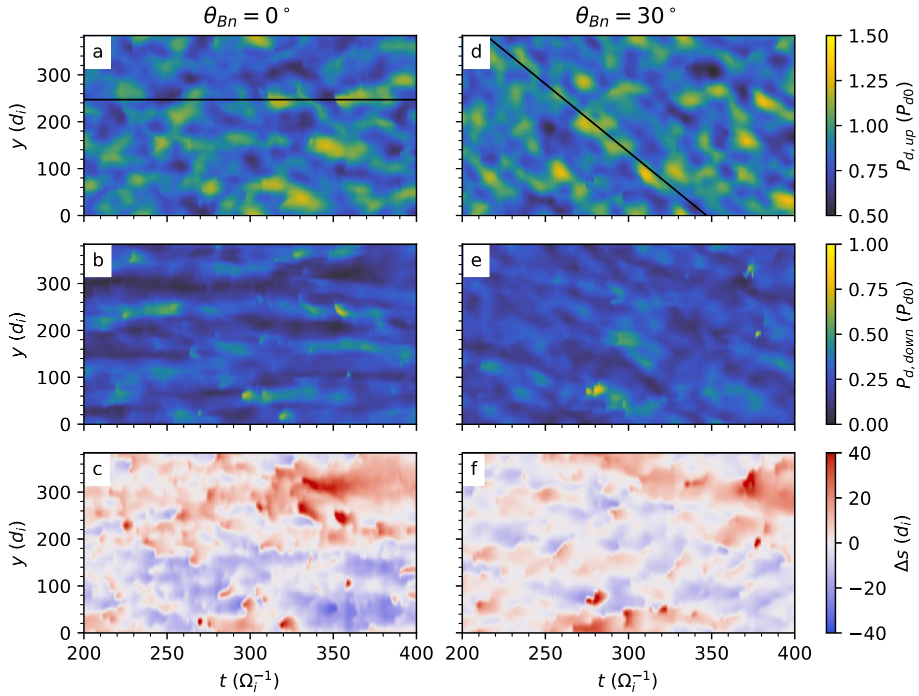

Figure 11. Time evolution of the dynamic pressure averaged in a 30 $d_i \times$ 30 d_i box with the center (a, d) 50 d_i upstream ($P_{d,\mathrm{up}}$) and (b, e) 20 d_i downstream ($P_{d,\mathrm{down}}$) from the shock front, and (c, f) the offset (Δs) of the shock front, obtained from (a–c) Case 7 and (d–f) Case 8. The quantities are normalized the same as in Figure 3. The black reference lines show the movement of the compressive structures (a, d).

4. With the increase of the shock angle θ_{Bn}, the sizes of downstream HSJs become smaller and their propagation speeds along the y direction become larger. Moreover, the dependency of the HSJ's scale size over plasma β becomes weaker.
5. The scale size of HSJs increases with increasing Mach number when other parameters are the same.

Hietala et al. (2009) proposed that HSJs downstream of a quasi-parallel shock are formed when the upstream plasma flow is deflected and suffers less deceleration when crossing through the inclined part of a rippled shock. Hao, Lembege, et al. (2016) attributed the formation of downstream HSJs to the interaction between the upstream plasma waves and the shock front. In this paper, we find that both the shock ripples and the downstream HSJs are the consequences of the compressive structures formed by upstream low-frequency waves. The interaction between the compressive structures and the shock front can generate the ripples at the shock front, and their enhanced densities can contribute to the increase of the downstream dynamic pressure. Meanwhile, the plasma flows have larger velocity in the downstream region of the dented parts of the shock front, which at last make the compressive structures evolve into HSJs.

Simultaneously, large-scale HSJs are usually observed in the magnetosheath, and they may trigger magnetic reconnection in the magnetopause (Karimabadi et al., 2014) and form throat aurora in the ionosphere (Han et al., 2016, 2017). With a 2-D global hybrid simulation, Guo et al. (2022) identified such kinds of large-scale HSJs downstream of a parallel shock. In this paper, we find that in a parallel shock, the interacting regions between the upstream compressive structures and the shock front remain unchanged, and the downstream HSJs can grow into large scales (Figure 12a). With the increase of the shock angle, the ripples and downstream HSJs propagate along the shock front, and the downstream HSJs can not grow into large sizes (Figure 12b).

This study utilizes a 2-D hybrid model to investigate the formation and evolution of HSJs. Although HSJs are 3-D structures and their evolution may involve physics along the z axis, the present 2-D simulations adequately elucidate the mechanism of the movement of the upstream compressive structure and HSJ along the y axis. To comprehensively investigate the 3-D structure and evolution of HSJs, further 3-D simulations are necessary.

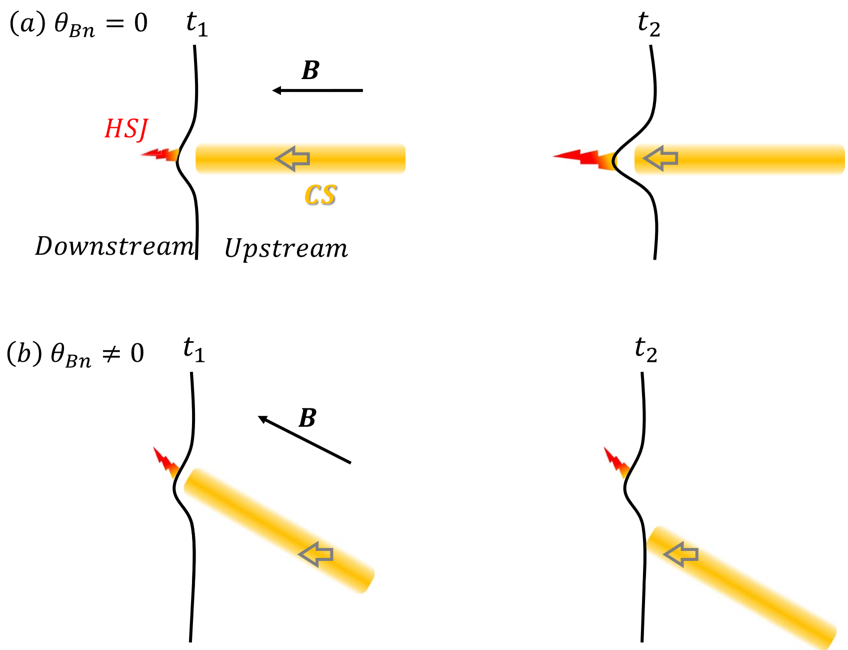

Figure 12. The sketch of the generation mechanism of large-scale high-speed jets (HSJs). When $\theta_{Bn} = 0°$ (a), the upstream compressive structures interact with the shock front in the same regions, deepen the shock ripples, and generate large-scale HSJs. When $\theta_{Bn} \neq 0°$ (b), the interacting regions move along the shock front, and the shock ripples and HJSs do not grow into large sizes.

Data Availability Statement

The authors gratefully acknowledge the data resources from the "National Space Science Data Center, National Science & Technology Infrastructure of China (www.nssdc.ac.cn)." The simulation data (Ren, 2023) used to plot the figures in this paper can be downloaded from https://doi.org/10.57760/sciencedb.07076.

Acknowledgments
This work was supported by NSFC Grant 42174181 and the Strategic Priority Research Program of Chinese Academy of Sciences Grant XDB41000000. Computer resources were provided by the Hefei Advanced Computing Center of China.

References

Archer, M. O., & Horbury, T. S. (2013). Magnetosheath dynamic pressure enhancements: Occurrence and typical properties. *Annales Geophysicae*, *31*(2), 319–331. https://doi.org/10.5194/angeo-31-319-2013

Archer, M. O., Horbury, T. S., & Eastwood, J. P. (2012). Magnetosheath pressure pulses: Generation downstream of the bow shock from solar wind discontinuities. *Journal of Geophysical Research*, *117*(A5), A05228. https://doi.org/10.1029/2011ja017468

Bale, S. D., Balikhin, M. A., Horbury, T. S., Krasnoselskikh, V. V., Kucharek, H., Möbius, E., et al. (2005). Quasi-perpendicular shock structure and processes. *Space Science Reviews*, *118*(1–4), 161–203. https://doi.org/10.1007/s11214-005-3827-0

Blanco-Cano, X., Omidi, N., & Russell, C. T. (2009). Global hybrid simulations: Foreshock waves and cavitons under radial interplanetary magnetic field geometry. *Journal of Geophysical Research*, *114*(A1), A01216. https://doi.org/10.1029/2008ja013406

Cao, J. B., Fu, H. S., Zhang, T. L., Reme, H., Dandouras, I., & Lucek, E. (2009). Direct evidence of solar wind deceleration in the foreshock of the Earth. *Journal of Geophysical Research*, *114*(A2), A02207. https://doi.org/10.1029/2008ja013524

Fu, H.-S., Cao, J.-B., Yang, B., Lucek, E., Rème, H., & Dandouras, I. (2009). ULF waves associated with solar wind deceleration in the Earth's foreshock. *Chinese Physics Letters*, *26*(11), 119402. https://doi.org/10.1088/0256-307x/26/11/119402

Gunell, H., Wieser, G. S., Mella, M., Maggiolo, R., Nilsson, H., Darrouzet, F., et al. (2014). Waves in high-speed plasmoids in the magnetosheath and at the magnetopause. *Annales Geophysicae*, *32*(8), 991–1009. https://doi.org/10.5194/angeo-32-991-2014

Guo, J., Lu, S., Lu, Q., Lin, Y., Wang, X., Ren, J., et al. (2022). Large-scale high-speed jets in Earth's magnetosheath: Global hybrid simulations. *Journal of Geophysical Research: Space Physics*, *127*(6), e2022JA030477. https://doi.org/10.1029/2022ja030477

Han, D.-S., Hietala, H., Chen, X.-C., Nishimura, Y., Lyons, L. R., Liu, J.-J., et al. (2017). Observational properties of dayside throat aurora and implications on the possible generation mechanisms. *Journal of Geophysical Research: Space Physics*, *122*(2), 1853–1870. https://doi.org/10.1002/2016ja023394

Han, D.-S., Nishimura, Y., Lyons, L. R., Hu, H.-Q., & Yang, H.-G. (2016). Throat aurora: The ionospheric signature of magnetosheath particles penetrating into the magnetosphere. *Geophysical Research Letters*, *43*(5), 1819–1827. https://doi.org/10.1002/2016gl068181

Hao, Y., Lembege, B., Lu, Q., & Guo, F. (2016). Formation of downstream high-speed jets by a rippled nonstationary quasi-parallel shock: 2-d hybrid simulations. *Journal of Geophysical Research: Space Physics*, *121*(3), 2080–2094. https://doi.org/10.1002/2015ja021419

Hao, Y., Lu, Q., Gao, X., & Wang, S. (2016). Ion dynamics at a rippled quasi-parallel shock: 2D hybrid simulations. *The Astrophysical Journal*, *823*(1), 7. https://doi.org/10.3847/0004-637x/823/1/7

Hao, Y., Lu, Q., Wu, D., Lu, S., Xiang, L., & Ke, Y. (2021). Low-frequency waves upstream of quasi-parallel shocks: Two-dimensional hybrid simulations. *The Astrophysical Journal*, *915*(1), 64. https://doi.org/10.3847/1538-4357/ac02ce

Hietala, H., Laitinen, T. V., Andréeová, K., Vainio, R., Vaivads, A., Palmroth, M., et al. (2009). Supermagnetosonic jets behind a collisionless quasiparallel shock. *Physical Review Letters*, *103*(24), 245001. https://doi.org/10.1103/physrevlett.103.245001

Hietala, H., Partamies, N., Laitinen, T. V., Clausen, L. B. N., Facskó, G., Vaivads, A., et al. (2012). Supermagnetosonic subsolar magnetosheath jets and their effects: From the solar wind to the ionospheric convection. *Annales Geophysicae*, *30*(1), 33–48. https://doi.org/10.5194/angeo-30-33-2012

Karimabadi, H., Roytershteyn, V., Vu, H. X., Omelchenko, Y. A., Scudder, J., Daughton, W., et al. (2014). The link between shocks, turbulence, and magnetic reconnection in collisionless plasmas. *Physics of Plasmas*, *21*(6), 062308. https://doi.org/10.1063/1.4882875

Karlsson, T., Kullen, A., Liljeblad, E., Brenning, N., Nilsson, H., Gunell, H., & Hamrin, M. (2015). On the origin of magnetosheath plasmoids and their relation to magnetosheath jets. *Journal of Geophysical Research: Space Physics*, *120*(9), 7390–7403. https://doi.org/10.1002/2015ja021487

Lembege, B., Giacalone, J., Scholer, M., Hada, T., Hoshino, M., Krasnoselskikh, V., et al. (2004). Selected problems in collisionless-shock physics. *Space Science Reviews*, *110*(3/4), 161–226. https://doi.org/10.1023/b%3Aspac.0000023372.12232.b7

Lembege, B., & Savoini, P. (1992). Nonstationarity of a two-dimensional quasiperpendicular supercritical collisionless shock by self-reformation. *Physics of Fluids B: Plasma Physics*, *4*(11), 3533–3548. https://doi.org/10.1063/1.860361

Leroy, M. M., Goodrich, C. C., Winske, D., Wu, C. S., & Papadopoulos, K. (1981). Simulation of a perpendicular bow shock. *Geophysical Research Letters*, *8*(12), 1269–1272. https://doi.org/10.1029/gl008i012p01269

Liu, Y. Y., Fu, H. S., Liu, C. M., Wang, Z., Escoubet, P., Hwang, K.-J., et al. (2019). Parallel electron heating by tangential discontinuity in the turbulent magnetosheath. *The Astrophysical Journal*, *877*(2), L16. https://doi.org/10.3847/2041-8213/ab1fe6

Lu, Q., Wang, H., Wang, X., Lu, S., Wang, R., Gao, X., & Wang, S. (2020). Turbulence-driven magnetic reconnection in the magnetosheath downstream of a quasi-parallel shock: A three-dimensional global hybrid simulation. *Geophysical Research Letters*, *47*(1), e2019GL085661. https://doi.org/10.1029/2019gl085661

Lu, Q. M., Xia, L. D., & Wang, S. (2006). Hybrid simulations of parallel and oblique electromagnetic alpha/proton instabilities in the solar wind. *Journal of Geophysical Research*, *111*(A9), A09101. https://doi.org/10.1029/2006ja011752

Němeček, Z., Šafránková, J., Přech, L., Sibeck, D. G., Kokubun, S., & Mukai, T. (1998). Transient flux enhancements in the magnetosheath. *Geophysical Research Letters*, *25*(8), 1273–1276. https://doi.org/10.1029/98gl50873

Omidi, N. (2007). Formation of cavities in the foreshock. In *AIP conference proceedings*. AIP. https://doi.org/10.1063/1.2778962

Omidi, N., Berchem, J., Sibeck, D., & Zhang, H. (2016). Impacts of spontaneous hot flow anomalies on the magnetosheath and magnetopause. *Journal of Geophysical Research: Space Physics*, *121*(4), 3155–3169. https://doi.org/10.1002/2015ja022170

Omidi, N., Zhang, H., Sibeck, D., & Turner, D. (2013). Spontaneous hot flow anomalies at quasi-parallel shocks: 2. Hybrid simulations. *Journal of Geophysical Research: Space Physics*, *118*(1), 173–180. https://doi.org/10.1029/2012ja018099

Palmroth, M., Hietala, H., Plaschke, F., Archer, M., Karlsson, T., Blanco-Cano, X., et al. (2018). Magnetosheath jet properties and evolution as determined by a global hybrid-vlasov simulation. *Annales Geophysicae*, *36*(5), 1171–1182. https://doi.org/10.5194/angeo-36-1171-2018

Plaschke, F., Hietala, H., & Angelopoulos, V. (2013). Anti-sunward high-speed jets in the subsolar magnetosheath. *Annales Geophysicae*, *31*(10), 1877–1889. https://doi.org/10.5194/angeo-31-1877-2013

Plaschke, F., Hietala, H., Angelopoulos, V., & Nakamura, R. (2016). Geoeffective jets impacting the magnetopause are very common. *Journal of Geophysical Research: Space Physics*, *121*(4), 3240–3253. https://doi.org/10.1002/2016ja022534

Plaschke, F., Hietala, H., Archer, M., Blanco-Cano, X., Kajdič, P., Karlsson, T., et al. (2018). Jets downstream of collisionless shocks. *Space Science Reviews*, *214*(5), 81. https://doi.org/10.1007/s11214-018-0516-3

Plaschke, F., Hietala, H., & Vörös, Z. (2020). Scale sizes of magnetosheath jets. *Journal of Geophysical Research: Space Physics*, *125*(9), e2020JA027962. https://doi.org/10.1029/2020ja027962

Preisser, L., Blanco-Cano, X., Kajdič, P., Burgess, D., & Trotta, D. (2020). Magnetosheath jets and plasmoids: Characteristics and formation mechanisms from hybrid simulations. *The Astrophysical Journal Letters*, *900*(1), L6. https://doi.org/10.3847/2041-8213/abad2b

Quest, K. B. (1988). Theory and simulation of collisionless parallel shocks. *Journal of Geophysical Research*, *93*(A9), 9649. https://doi.org/10.1029/ja093ia09p09649

Raptis, S., Karlsson, T., Vaivads, A., Pollock, C., Plaschke, F., Johlander, A., et al. (2022). Downstream high-speed plasma jet generation as a direct consequence of shock reformation. *Nature Communications*, *13*(1), 598. https://doi.org/10.1038/s41467-022-28110-4

Ren, J. (2023). Data for two-dimensional hybrid simulations of high-speed jets downstream of quasi-parallel shocks (Version 2) [Dataset]. Science Data Bank. https://doi.org/10.57760/SCIENCEDB.07076

Savin, S., Amata, E., Zelenyi, L., Lutsenko, V., Safrankova, J., Nemecek, Z., et al. (2012). Super fast plasma streams as drivers of transient and anomalous magnetospheric dynamics. *Annales Geophysicae*, *30*(1), 1–7. https://doi.org/10.5194/angeo-30-1-2012

Scholer, M. (2003). Short large-amplitude magnetic structures and whistler wave precursors in a full-particle quasi-parallel shock simulation. *Journal of Geophysical Research*, *108*(A7), 1273. https://doi.org/10.1029/2002ja009820

Schwartz, S. J. (1991). Magnetic field structures and related phenomena at quasi-parallel shocks. *Advances in Space Research*, *11*(9), 231–240. https://doi.org/10.1016/0273-1177%2891%2990039-m

Schwartz, S. J., & Burgess, D. (1991). Quasi-parallel shocks: A patchwork of three-dimensional structures. *Geophysical Research Letters*, *18*(3), 373–376. https://doi.org/10.1029/91gl00138

Su, Y., Lu, Q., Huang, C., Wu, M., Gao, X., & Wang, S. (2012). Particle acceleration and generation of diffuse superthermal ions at a quasi-parallel collisionless shock: Hybrid simulations. *Journal of Geophysical Research*, *117*(A8), A08107. https://doi.org/10.1029/2012ja017736

Suni, J., Palmroth, M., Turc, L., Battarbee, M., Johlander, A., Tarvus, V., et al. (2021). Connection between foreshock structures and the generation of magnetosheath jets: Vlasiator results. *Geophysical Research Letters*, *48*(20), e2021GL095655. https://doi.org/10.1029/2021gl095655

Tsubouchi, K., & Lembège, B. (2004). Full particle simulations of short large-amplitude magnetic structures (SLAMS) in quasi-parallel shocks. *Journal of Geophysical Research*, *109*(A2), A02114. https://doi.org/10.1029/2003ja010014

Veselovsky, I. S., Dmitriev, A. V., & Suvorova, A. V. (2010). Algebra and statistics of the solar wind. *Cosmic Research*, *48*(2), 113–128. https://doi.org/10.1134/s0010952510020012

Wang, B., Nishimura, Y., Hietala, H., Lyons, L., Angelopoulos, V., Plaschke, F., et al. (2018). Impacts of magnetosheath high-speed jets on the magnetosphere and ionosphere measured by optical imaging and satellite observations. *Journal of Geophysical Research: Space Physics*, *123*(6), 4879–4894. https://doi.org/10.1029/2017ja024954

Wu, M., Hao, Y., Lu, Q., Huang, C., Guo, F., & Wang, S. (2015). The role of large amplitude upstream low-frequency waves in the generation of superthermal ions at a quasi-parallel collisionless shock: *Cluster* observations. *The Astrophysical Journal*, *808*(1), 2. https://doi.org/10.1088/0004-637x/808/1/2

Yang, Z. W., Lembège, B., & Lu, Q. M. (2012). Impact of the rippling of a perpendicular shock front on ion dynamics. *Journal of Geophysical Research*, *117*(A7). https://doi.org/10.1029/2011ja017211

Yang, Z. W., Lu, Q. M., Lembège, B., & Wang, S. (2009). Shock front nonstationarity and ion acceleration in supercritical perpendicular shocks. *Journal of Geophysical Research*, *114*(A3), A03111. https://doi.org/10.1029/2008ja013785

Zhang, H., Sibeck, D. G., Zong, Q.-G., Omidi, N., Turner, D., & Clausen, L. B. N. (2013). Spontaneous hot flow anomalies at quasi-parallel shocks: 1. Observations. *Journal of Geophysical Research: Space Physics*, *118*(6), 3357–3363. https://doi.org/10.1002/jgra.50376